COMSOL
CONFERENCE
2023 MUNICH

# A 2D Computational Model of an Active Magnetocaloric Regenerator with Parallel Plates

Francisco Rodríguez-Méndez[1], Bruno Chinè[1], Simone Fabbrici[2], Franca Albertini[2], Daniela Negri[3], Francesco Cugini[4], Massimo Solzi[4]

1. School of Materials Science and Engineering, Costa Rica Institute of Technology, Cartago, Costa Rica.
2. Institute of Materials for Electronics and Magnetism, National Research Council, Parma, Italy.
3. Independent Researcher, Fidenza, Italy.
4. Department of Mathematical, Physical and Computer Sciences, University of Parma, Italy.

## Abstract

In this work, a 2-dimensional time-dependent model of a magnetic refrigeration system with an active magnetic regenerator (AMR) is developed using COMSOL Multiphysics®. The model consists of a regenerator with parallel plates, hot and cold heat exchangers, and a working fluid. It uses experimental measurements of $\Delta T_{ad}(H,T)$ and $c_p(H,T)$ as an input to account for the MCE, later providing characteristic response metrics of the cooling system such as the temperature span, pressure difference, field fluid velocity and cooling power. With this approach, three different magnetocaloric materials (MCM) were investigated – $Ni_{49.6}Mn_{34.2}In_{16.1}$, and $Ni_{50}Mn_{35}In_{15}$ Heusler compounds, and Gd – with direct and inverse MCE, where most of the important operation conditions of the system remained fixed, for instance, fluid flow rate, working frequency, magnetic field strength, and number and dimensions of the plates. The results indicate that Gd performs better than the other two materials in terms of cooling capacity and temperature span, being the $Ni_{49.6}Mn_{34.2}In_{16.1}$ alloy the one that generates the lowest performance. Even though the Heusler compounds did not perform as well as the Gd, this model encourages future studies where the working parameters of the magnetic refrigeration system can be varied to enhance and optimize the performance of these MCMs and overall, the response of the thermo-magnetic device.

**Keywords:** magnetocaloric materials, magnetic refrigeration, computational modeling and simulation, non-isothermal flow, heat transfer, fluid dynamics.

## Introduction

Around 17% of the primary energy produced worldwide is consumed by refrigeration and air conditioning systems [1] [2], reaching a power intake of 2000 TWh, approximately [3]. Furthermore, these thermal management devices are based on vapor compression technologies, which still use refrigerants with a high greenhouse effect potential, such as fluorocarbons and carbon dioxides, contributing with the 7.8% emissions of greenhouse gases to the atmosphere [4] [5]. Therefore, as an energy-efficient and environmental-friendly alternative, magnetic refrigeration is considered one of the best emergent technologies to replace vapor compression plants [6].

Compared with modern cooling systems, magnetic refrigeration uses a solid material as a refrigerant, which exhibits zero ozone depletion and global warming potential. On the other hand, it can also reach efficiencies up to 60% of the Carnot cycle, against the 40% of the best options currently available on the market [7], obtaining the potential ability to reduce energy consumption by up to 20%-30% [8].

Magnetic refrigeration technology is based on the magnetocaloric effect (MCE). This phenomenon occurs when a material with magnetic properties is exposed to a magnetic field, resulting in a change in its magnetic order and a consequent decrease in the entropy of the magnetic contribution. Under isentropic conditions, the total entropy of the material remains constant [9], therefore, the change in the magnetic entropy is compensated by a change in the lattice entropy, which results in an adiabatic temperature change $\Delta T_{ad}$ of the material [10] [11]. When the material experiences an increase in its temperature under the application of a magnetic field, the MCE is called direct, but if the material cools down, then it is defined as an inverse MCE [12].

Nowadays, there are many research prototypes using the principle of magnetic refrigeration to obtain a competitive thermal span and cooling power [13], but still no commercial products are available. For this new technology to have a niche in the market, significant work must be done in the field of materials science, specifically in the processing and manufacturing of magnetocaloric materials with better properties [14] [15]. Among the most critical requirements, both the adiabatic temperature and entropy changes of the material must be as large as possible in small magnetic field variations, as they are directly related to the temperature span of the device and the quantity of heat that can be transferred in one cooling cycle [16] [17], respectively.

The benchmark material with the best properties is gadolinium (Gd), which has been used in most of the magnetocaloric devices [18] [19]. But since Gd is a heavy rare-earth with low availability and high cost, alternative rare-earth-free materials are the subject of current research. Ni-Mn-based Heusler alloys are low cost, recyclable, highly available, and rare-earth

free, making them a promising material for magnetic refrigeration applications. However, many of them exhibit low adiabatic temperature change under cycling due to a large thermal hysteresis [20] [21] [22]. In the other hand, the material adiabatic temperature change alone is not sufficient to achieve the temperatures required for most refrigeration applications – $\Delta T_{ad}$ of Gd at 1T magnetic field is only ~3K, for example. To expand this operating range, the principle of an active magnetic regenerator (AMR) is used. An AMR is a structure composed of a magnetocaloric material through which a fluid is pumped in the opposite direction to the heat flow. This regenerator has a double function, as it plays the role of both a cooling element and a heat regenerator [23]. Therefore, to generate a large temperature gradient, the operation of the AMR must ensure that the fluid keeps cycling from a cold end to a hot end of the device, taking the heat load and transferring it to the environment [24]. A full cycle, which is also known as the Brayton refrigeration cycle [25], consists in four different steps, as also shown in Fig. 1:

a) *Magnetization* of the AMR as it is exposed to the magnetic field, resulting in the increment of the temperature of each piece of the MCM.
b) *Fluid flow* from the cold end through the heated MCM to the hot end, where the heat received from the MCM is transmitted to the environment.
c) *Demagnetization* of the AMR as the magnetic field is removed, resulting in the decrease of the temperature of each piece of the MCM.
d) *Fluid flow* from the hot end through the cooled MCM (where the fluid is cooled) to the cold end, where the heat is absorbed from the surroundings (the refrigerator chamber).

Several computational studies have been carried out to assess the performance of this AMR cycle using various magnetocaloric materials. Tusek et al. [26] used Gd in a packed-bed regenerator and found that smaller spheres yielded larger cooling capacity due to better heat transfer properties. Tomc [27] reported the first method for optimizing the minimum number of layers necessary to increase the performance of an AMR with parallel plates. Trevizoli et al. [28] [29] developed a computational model that also uses an AMR with a packed-bed of spheres, concluding that in order to increase the precision of the simulations the irreversibility of the internal heat transfer of the system, viscous losses of the working fluid, losses due to the demagnetization phase, and heat losses to the environment must be taken into account. Zhang et al. [30] used modeling and simulation techniques to optimize the length of the AMR layers manufactured with different LaFeMnSiH compounds. They found that the best performance of the regenerator occurred at a frequency of 0.1Hz with a layer length of 200mm, obtaining a simulated span temperature of 41K. Aprea et al. [2] [31] assessed six different AMRs, demonstrating that parallel plates regenerators have greater efficiency, but only if the plates are perfectly parallel, being the packed-bed of spheres the most viable option for real applications.

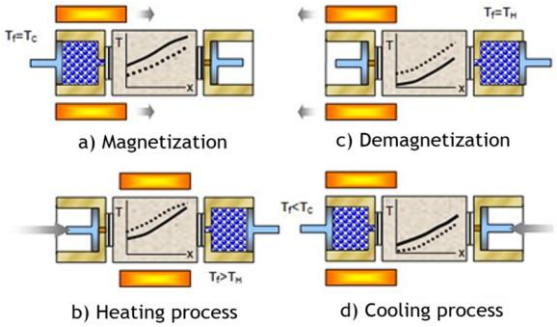


***Figure 1.*** *Phases of the Brayton refrigeration cycle.*

This work aims to study the performance of three different MCMs – $Ni_{49.6}Mn_{34.2}In_{16.1}$, and $Ni_{50}Mn_{35}In_{15}$ Heusler compounds, and Gd – in an AMR cycle by building a robust computational model in COMSOL Multiphysics®. This approach, as shown in Fig. 2, uses a complete set of parallel plates as regenerator, cold and hot heat exchangers (CHEX and HHEX, respectively), and a working fluid. The model has a fixed geometry and operates with constant values for fluid velocity, cycle period, and magnetic field, but changes the system initial temperature to match the temperature of each MCM studied at which the MCE is maximized (Curie temperature). The $\Delta T_{ad}$ and heat capacities of the materials are measured experimentally rather than mean field approximations, and the fluid motion considers viscous losses. Main metrics used to evaluate the magnetic device performance are the maximum temperature span obtained, the cooling capacity at no-load condition, and the coefficient of performance (COP).

## AMR Modeling

The model is based on the COMSOL Multiphysics® Conjugate Heat Transfer module that combines the Heat Transfer in Solids and Fluids and the Laminar Flow physics under the Non-Isothermal Flow Multiphysics interface. The dependent variables, such as fluid pressure and velocity, and temperature distribution across the AMR, are solved using the Finite Element Method. Therefore, the velocity and pressure profiles are first determined along the fluid and then they are used to solve the temperature distribution in both the solid and fluid domains during the cold and hot fluid flows, respectively. This process is repeated for several cooling cycles for the system to reach a steady-state condition.

### Governing equations of the model

Assuming the fluid flow is laminar, the velocity distribution in the fluid is determined by solving the Navier-Stokes momentum and continuity equations

$$\rho_f \left(\frac{\partial U}{\partial t} + (U \cdot \nabla)U\right) - \mu_f \nabla^2 U + \nabla p = 0 \quad (1)$$

$$\nabla \cdot U = 0 \quad (2)$$

where $\rho_f$ is the density of the fluid, $\mu_f$ is the dynamic viscosity of the fluid, $U$ is the fluid velocity field, $p$ is the pressure, and $t$ is time.

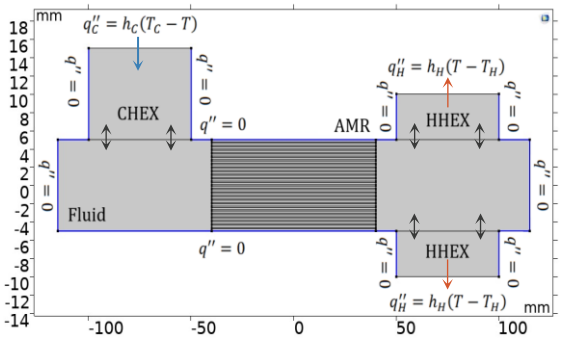


***Figure 2.*** *AMR model and boundary conditions used.*

Then, the temperature distribution in the solid regenerator and the heat exchangers domains is calculated by solving the equation

$$\rho_s c_{p,s} \frac{\partial T_s}{\partial t} - k_s \nabla^2 T_s = \dot{Q}_{MCE} + \dot{Q}_{HT} \qquad (3)$$

where $c_{p,s}$ is the specific heat capacity of the solid, $T_s$ is the solid temperature, and $k_s$ is the solid thermal conductivity. Here, the MCE is introduced in the term $\dot{Q}_{MCE}$ as a heat source in the energy equation and defined as a function of the $\Delta T_{ad}(H,T)$ with respect to time, and the $c_p(H,T)$ of the MCM. Is it important to note that both $\Delta T_{ad}(H,T)$ and $c_p(H,T)$ are dependent on the applied magnetic field and the instant temperature of the regenerator. The relation that describes this effect is calculated by

$$\rho_s c_p(H,T) \frac{\Delta T_{ad}(H,T)}{dt} = \dot{Q}_{MCE} \qquad (4)$$

$\Delta T_{ad}(H,T)$ and $c_p(H,T)$ parameters are introduced in the model by using interpolated functions based on experimental data for each of MCM studied, as illustrated in Figs. 3 and 4, where the $Ni_{50}Mn_{35}In_{15}$ $\Delta T_{ad}$ data was measured in [32], and its $c_p$ values are based on measurements found in [33].

Besides, it is worth noting that unlike $Ni_{50}Mn_{35}In_{15}$ and Gd, which manifest conventional MCE at their Curie transition temperature, the $Ni_{49.6}Mn_{34.2}In_{16.1}$ Heusler alloy exhibit a thermal hysteresis caused by the first-order ferromagnetic-to-paramagnetic transition that takes place at its martensitic phase transformation. This characteristic not only affects the material $\Delta T_{ad}$ cycling behavior, as it is shown in the Fig. 3, where one curve describes the MCM heating phase and a different one the cooling process, but also displaying an inverse MCE near 300K.

Subsequently, the heat transfer for incompressible fluids with convective terms, with the $\dot{Q}_{HT}$ term linking the solid and fluid domains, is calculated by the next equation

$$\rho_f c_{p,f} \left( \frac{\partial T_f}{\partial t} + (U \cdot \nabla) T_f \right) - k_f \nabla^2 T_f = -\dot{Q}_{HT} \qquad (5)$$

where $c_{p,f}$ is the specific heat capacity of the fluid, $T_f$ is the fluid temperature, and $k_f$ is the fluid thermal conductivity. The velocity field calculated in Eqs. (1) and (2) are used in equation (5) to determine the convective heat transfer.

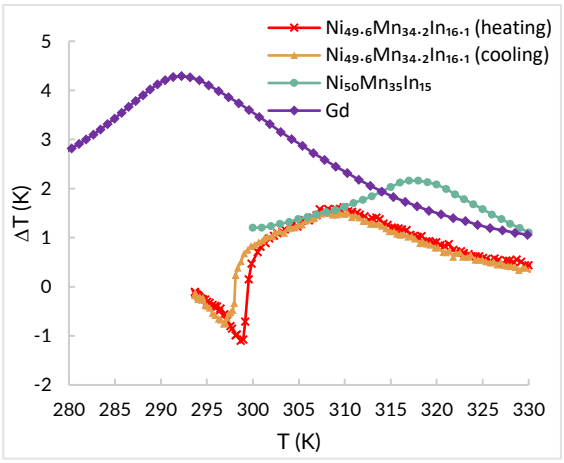


***Figure 3.*** *$\Delta T_{ad}$ for each magnetocaloric material used under a magnetic field change of 1.8T.*

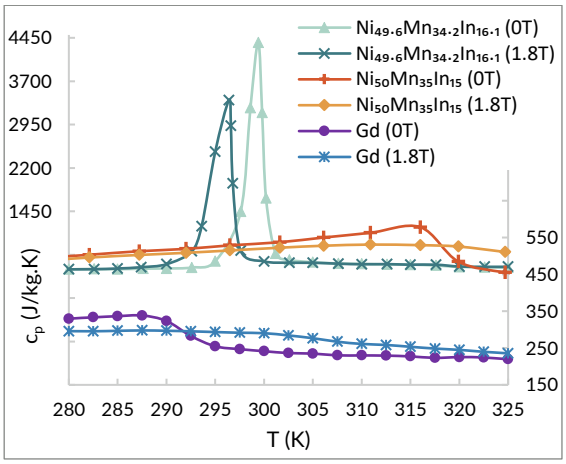


***Figure 4.*** *Specific heat values, for each magnetocaloric material used under a magnetic field of 0T and 1.8T.*

**Boundary conditions and design parameters of the AMR model**

The regenerator in the model is made of the MCM, the cold and hot heat exchangers are built of copper, and the heat transfer fluid is pure water. As shown in Fig. 2, external boundaries have adiabatic conditions imposed on them, except for the outward boundaries of CHEX and HHEX, which have a prescribed heat flux. The solid domains and the fluid are assumed to be in perfect contact following the boundary condition given in the relation

$$\left(k_f \frac{\partial T_f}{\partial y}\right)\Big|_{y=H_{fl}} = \left(k_s \frac{\partial T_s}{\partial y}\right)\Big|_{y=H_{fl}} \qquad (6)$$

Also, in each fluid-solid interface, the "no-slip wall" condition has been imposed.

The geometrical configuration implemented in the model is summarized in Table 1, where a total of 26 parallel plates were built into the regenerator. For the Brayton refrigeration cycle described in the introduction, the time steps for the four stages are symmetrically distributed. This parameter along others of equally importance, such as the strength of the magnetic field, the cycle period, the fluid velocity in the fluid flows phases, the initial prime temperature for each MCM, and the heat transfer coefficients for

***Table 1.*** *Geometrical configuration of the model.*

| Part | Dimensions (mm$^2$) |
|---|---|
| Regenerator plates | 80 x 0.25 |
| Cold heat exchanger | 50 x 10 |
| Hot heat exchanger | 50 x 5 |
| Fluid channel | 230 x 14 |
| Heat exchanger-regenerator gap | 10 |
| Gap between plates | 0.01 |

the outward boundaries of the heat exchangers are provided in Table 2. For the latter parameter, perfect thermal contact between the hot heat exchanger and the outside environment is assumed by making the value of the heat transfer coefficient in the outward boundary of the hot end very large. In the other hand, to assess the performance of the regenerator at maximum cooling capacity, the heat transfer coefficient at the CHEX is set to 0 W/(m$^2$.K), i.e. no cooling-load is considered in this simulation.

### Performance evaluation metrics

The assessment of the performance of the system is determined by the temperature span achieved for the device, and the cooling capacity. $\Delta T_{span}$ is the temperature difference between the hot and cold heat exchangers. Then, for the cooling capacity, the amount of cooling per cycle absorbed is determined by the integration of the heat flux through the outward boundary of the CHEX as follows

$$q_c' = \int_0^{\tau}\int_0^{L_{HEX}} \dot{q}_c'' \, dxdt \tag{7}$$

where $\tau$ is the cycle period and $L_{HEX}$ is the length of the heat exchanger. The corresponding refrigeration capacity per cycle is now calculated by the relation

$$\dot{q}_c' = \frac{q_c'}{\tau} \tag{8}$$

Derived from the cooling capacity, we can also calculate the coefficient of performance (COP) of the system. First, the rejected heat per cycle is determined by the integration of the heat flux through the outer boundary of the HHEX as follows

$$q_r' = \int_0^{\tau}\int_0^{L_{HEX}} \dot{q}_r'' \, dxdt \tag{9}$$

Then, the total work done by the AMR is the sum of the work required to magnetize the regenerator and the work required to displace the fluid

$$w_{tot}' = w_{mag}' + w_{pump}' \tag{10}$$

The work required to magnetize and demagnetize the regenerator can be calculated with the equation

$$w_{mag}' = q_r' + q_c' \tag{11}$$

The pressure drop in the regenerator is then needed to calculate the pumping power required to move the working fluid through the AMR. Generally, the relationship between these two variables is described by

$$\dot{w}_{pump} = \frac{U_f \nabla p}{\eta_{pump}} \tag{12}$$

***Table 2.*** *Initial and working conditions of the model.*

| Parameter | Value |
|---|---|
| Magnetic field strength | 1.8T |
| Total cycle period | 2s |
| Fluid flows step time | 1s |
| (de)magnetization step time | 1s |
| Fluid velocity | 0.024 m/s |
| Heat flux CHEX ($h_C$) | 0 W/(m$^2$.K) |
| Heat flux HHEX ($h_H$) | 10E3 W/(m$^2$.K) |
| $Ni_{49.6}Mn_{34.2}In_{16.1}$ initial temperature | 298K |
| $Ni_{50}Mn_{35}In_{15}$ initial temperature | 316K |
| Gd initial temperature | 292K |

where $\eta_{pump}$ is the pump efficiency, assumed to be around 0.8 for most devices.
Finally, the COP of the AMR is calculated by

$$COP = -\frac{q_c'}{w_{tot}'} \tag{13}$$

## Simulation Results and Discussion

### MCMs assessment

Fig. 5 illustrates the development of the $\Delta T$ over time for (a) $Ni_{49.6}Mn_{34.2}In_{16.1}$, (b) $Ni_{50}Mn_{35}In_{15}$, and (c) Gd materials, respectively. For each simulation, 600 cycles were performed, which is equivalent to 1200s with a time step of 0.1s. As expected, the Gd is capable of build a larger AMR $\Delta T$ than the Heusler compounds studied, due to its bigger $\Delta T_{ad}$. It is also noticeable that, for the total cycles simulated, the Gd and $Ni_{50}Mn_{35}In_{15}$ do not arrive to a steady-state condition, where the $\Delta T$ between two consecutive cycles is equal or less than 0.01K, meaning we need to increase the study number of cycles until the above condition is fulfilled. Meanwhile, $Ni_{49.6}Mn_{34.2}In_{16.1}$ reached a steady-state in about 200s.
Here, the behavior of $Ni_{49.6}Mn_{34.2}In_{16.1}$ alloy is worth a closer look. As it displays an inverse MCE under 300K along with a thermal hysteresis, the hot part of the system is uncapable of building a positive temperature difference with the surroundings. This means that the device is no longer a cooling system, but a heat pumping one, since the temperature difference between the hot side of the AMR and the surrounddings now allows heat to enter the regenerator. To avoid this situation, better understanding of the inverse MCE and the thermal hysteresis of the material is needed, together with a study of another operation conditions, for example, dual magnet configuration with half the regenerator magnetized at half a cycle with the other half demagnetized, and different initial conditions, such as the working frequency, or the fluid volume displaced in one cycle.
Fig. 6 shows the 2D temperature evolution across the entire magnetic device during the (a) cold and (b) hot blow steps of the Brayton cycle described. For convenience, the images were taken using the Gd as the model material. In the cold blow step of the cooling cycle, the heat generated in the AMR due to the MCE is transferred into the working fluid and moved towards the HHEX, where it will heat up the hot side

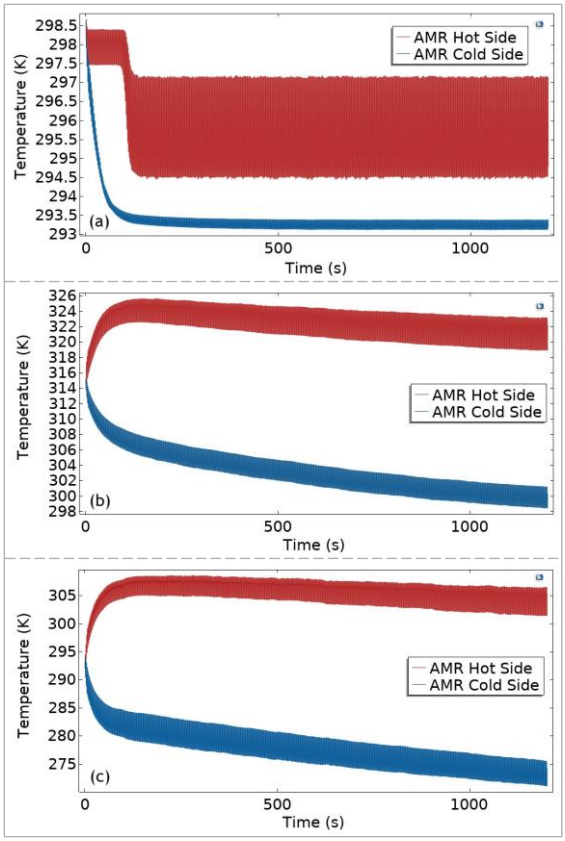


***Figure 5.*** *ΔT behavior over time at the hot and cold ends of the AMR for (a) $Ni_{49.6}Mn_{34.2}In_{16.1}$, (b) $Ni_{50}Mn_{35}In_{15}$, and (c) Gd materials.*

of the system. The other way around, during the hot blow phase, after the regenerator is demagnetized, the temperature of the fluid is reduced by the colder AMR. Then, the cooled fluid is transferred towards the CHEX, reducing the temperature of the cold side of the system.

### Performance Evaluation

Three metrics are used to evaluate the MCMs studied in the simulations: first, the $\Delta T_{span}$ between the cold and hot heat exchangers of the system; and second and third, the cooling power and the coefficient of performance COP at no-load.

For the latter two parameters, as stated in Eq. 12, the pressure losses along the AMR and the fluid velocity are needed. Fig. 7 show the (a) change in pressure across the regenerator, (b) the velocity profile during the hot and cold fluid blows, and (c) the 2D velocity distribution in the AMR. Pressure losses remain low – ~3360Pa – due to the geometry of the AMR and the perfect alignment between the parallel plates. In a real regenerator, ensuring that each plate is perfectly aligned is a difficult task to accomplish, leading to major pressure losses, vortex generation in the fluid, and temperature maldistribution.

Velocity profiles display a huge change in its value when the fluid enters the regenerator channels. This behavior obeys Bernoulli's principle as the area is drastically reduced coupled with the change in the pressure. As the fluid velocity along the channel is a

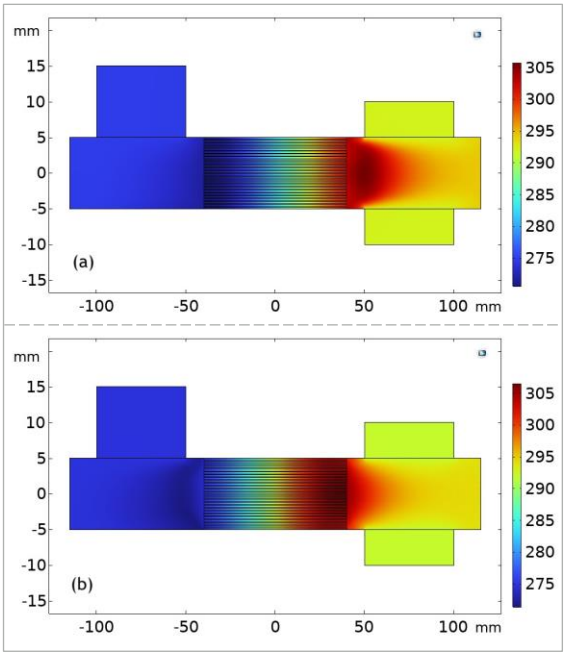


***Figure 6.*** *Temperature gradient across the AMR during (a) hot blow and (b) cold blow phases.*

key parameter that directly determines the efficacy of the AMR, further study on finding the optimal value of this variable is needed, since if the fluid velocity is too slow, the cooling effect of the MCM is not fully utilized, but if it is too high, the CHEX will absorb heat coming from the HHEX as well as the outside environment. In the simulations performed, with a fluid velocity inside the channels near 0.08m/s the amount of fluid displaced through the channels in each cycle is 30% of the fluid inside the AMR.

Obtained $\Delta T_{span}$, cooling capacity, and COP values are summarized in Table 3. The first thing to note is the COP negative value of $Ni_{49.6}Mn_{34.2}In_{16.1}$, which is explained with the fact exposed before, the AMR working with this martensitic Heusler compound functions as a heat pumping device instead of a cooling system. Besides this behavior, its cooling capacity and $\Delta T_{span}$ are the lowest if compared with the values achieved by the $Ni_{50}Mn_{35}In_{15}$ and the Gd. Now, the Gd performs better in terms of $\Delta T_{span}$ and cooling power calculated, but the $Ni_{50}Mn_{35}In_{15}$ alloy does not fall far from it, in fact, its numbers follow

***Table 3.*** *Performance parameters for all MCMs.*

| Parameter | Value |
|---|---|
| *$Ni_{49.6}Mn_{34.2}In_{16.1}$* | |
| Temperature span | 4.5K |
| Cooling capacity | 151.05W |
| Coefficient of performance | -1.05 |
| *$Ni_{50}Mn_{35}In_{15}$* | |
| Temperature span | 14.89K |
| Cooling capacity | 847.81W |
| Coefficient of performance | 1.80 |
| *Gadolinium* | |
| Temperature span | 17.25K |
| Cooling capacity | 974.78W |
| Coefficient of performance | 0.79 |

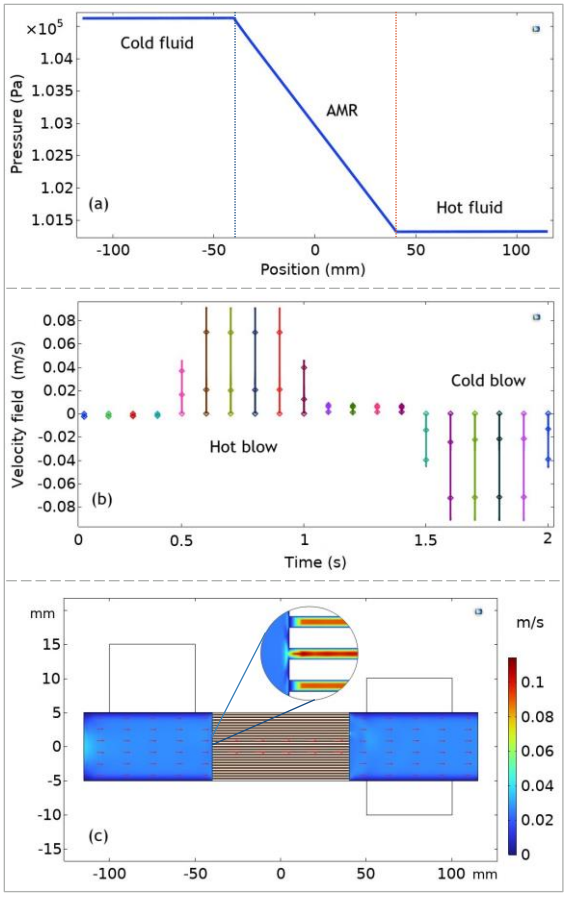


***Figure 7.*** *AMR (a) pressure losses, (b) fluid velocity in channels during hot and cold blow phases, and (c) 2D velocity profile during the fluid flows.*

closely the overall capabilities of Gd, with a $\Delta T_{span}$ and cooling power difference between them of about 2.3K and 125W, respectively. For COP metric, the $Ni_{50}Mn_{35}In_{15}$ Heusler compound has a higher value than the Gd. This means that $Ni_{50}Mn_{35}In_{15}$ displays a higher ratio of useful cooling provided to work required, which can be translated to the factor that this magnetocaloric material has lower energy consumption and the highest efficiency of all three MCMs analyzed here, but still falling behind if compared with most air conditioners (which have COP values of 2.3 to 3.5, approximately), for example.

Nevertheless, the performance responses achieved by the $Ni_{50}Mn_{35}In_{15}$ have the potential to make this material a preferable alternative over Gd considering the abundancy and cost of its constituent elements. One drawback we must consider with this Heusler compound is that the metrics obtained were calculated at its prime temperature (i.e., its Curie transition temperature), which is around 316K, meanwhile Gd works near room temperature ~292K. Therefore, the applications where this material will find its usefulness fall into industrial processes and perhaps electrical/electronic devices. Another possibility is to carry out a proper tuning of the elemental composition of this Heusler compound, with the purpose of shifting its Curie transition temperature closer to room temperature, while preserving its magnetocaloric behavior and performance response.

## Conclusions

This work presents a two-dimensional model of an active magnetocaloric regenerator built with parallel plates made of magnetocaloric materials. The model approach utilizes three different MCMs as refrigerants and calculates its performance response in terms of $\Delta T_{span}$, cooling capacity, and COP achieved at no load. The simulations show that the martensitic compound $Ni_{49.6}Mn_{34.2}In_{16.1}$ has an undesirable behavior as it acts as a pumping heat device due to its intrinsic inverse MCE and thermal hysteresis, also demonstrating the lowest $\Delta T_{span}$ and cooling power if compared with the other materials. Proper modifications to the operative conditions must be considered to exploit this material in a magnetocaloric machine. Gd is able to generate the largest $\Delta T_{span}$ and cooling power but followed closely by $Ni_{50}Mn_{35}In_{15}$, with a $\Delta T_{span}$ of about 15K and a cooling capacity of approximately 847.81W. Also, $Ni_{50}Mn_{35}In_{15}$ has the highest efficiency (COP), which makes it a viable option with great cost effectiveness, but for applications working near 316K. However, the results obtained encourage future analysis where different parameters of the model can be varied with the purpose of finding the optimal working conditions for every magnetocaloric material studied.

## Acknowledgements

The first two authors gratefully acknowledge the financial aid provided by the Vicerrectoría de Investigación y Extensión of the Instituto Tecnológico de Costa Rica, through the project 5402-1351-2301.

## References

[1] D. Coulomb, J. L. Dupont and A. Pichard, "The Role of Refrigeration in the Global Economy," 29th Informatory Note on Refrigeration Technologies, Technical Report, International Institute of Refrigeration, Paris, France, 2015.

[2] C. Aprea, A. Greco, A. Maiorino and C. Masselli, "Analyzing the energetic performances of AMR regenerator working with different magnetocaloric materials: Investigations and viewpoints," *International Journal of Heat and Technology*, vol. 35, no. 1, pp. S383-S390, 2017.

[3] International Energy Agency, "The Future of Cooling," 2018. [Online]. Available: http://www.iea.org/reports/the-future-of-cooling. [Accessed July 2023].

[4] D. Coulomb, J.-L. Dupont and V. Morlet, "The Impact of the Refrigeration Sector on Climate Change," 35th Informatory Note on Refrigeration Technologies, Technical Report, International Institute of Refrigeration, Paris, France, 2016.

[5] Y. Hwang, "Harmonization of the Life Cycle Climate Performance Methodology," 32nd Informatory Note on Refrigeration Technologies, International Institute of Refrigeration, Paris, France, 2016.

[6] A. Kitanovski, U. Plaznik, U. Tomc and A. Poredos, "Present and future caloric refrigeration and heatpump technologies," *International Journal of Refrigeration*, vol. 57, pp. 288-298, 2015.

[7] E. Brück, O. Tegus, O. Tegus, D. Thanh and K. Buschow, "Magnetocaloric refrigeration near room temperature," *Journal of Magnetism and Magnetic Materials*, vol. 310, no. 2, pp. 2793-2799, 2007.

[8] D. Velázquez, C. Estepa, E. Palacios and R. Burriel, "A comprehensive study of a versatile magnetic refrigeration demostrator," *International Journal or Refrigeration*, vol. 63, pp. 14-24, 2016.

[9] S. Choi, U. Han, H. Cho and H. Lee, "Review: Recent advances in household refrigerator cycle technologies," *Applied Thermal Engineering*, no. 132, pp. 560-574, 2018.

[10] V. K. Pecharsky and K. A. G. Jr, "Magnetocaloric effect and magnetic refrigeration," *Journal of Magnetism and Magnetic Materials*, vol. 1, no. 3, pp. 44-56, 1999.

[11] A. Tishin and Y. Spichkin, The Magnetocaloric Effect and its Applications, Boca Raton: CRC Press, 2003.

[12] T. Gottschall, "On the magnetocaloric properties of Heusler compounds: Reversible, time- and size-dependent effects of the martensitic phase transition," TUprints - TU Darmstadt publication service, Darmstadt, 2016.

[13] A. Greco, C. Aprea, A. Maiorino and C. Masselli, "A review of the state of the art of solid-state caloric cooling processes at room-temperature before 2019," *International Journal of Refrigeration*, vol. 106, p. 66–88, 2019.

[14] T. Gottschall, K. P. Skokov, M. Fries, A. Taubel, I. Radulov, F. Scheibel, D. Benke, S. Riegg and O. Gutfleisch, "Making a Cool Choice: The Materials Library of Magnetic Refrigeration," *Advanced Energy Materials*, vol. 9, no. 34, 2019.

[15] A. Kitanovski, "Energy Applications of Magnetocaloric Materials," *Advanced Energy Materials*, vol. 10, no. 10, 2020.

[16] J. Romero Gómez, R. Ferreiro Garcia, A. De Miguel Catoira and M. Romero Gómez, "Magnetocaloric effect: A review of the thermodynamic cycles in magnetic refrigeration," *Renewable and Sustainable Energy Reviews, Elsevier*, vol. 17, no. C, pp. 74-82, 2013.

[17] K. P. Skokov, A. Y. Karpenkov, D. Y. Karpenkov and O. Gutfleisch, "The maximal cooling power of magnetic and thermoelectric refrigerators with La(FeCoSi)13 alloys," *Journal of Applied Physics*, vol. 113, 2013.

[18] M. Balli, O. Sari, C. Mahmed, C. Besson, and J. Forchelet, "A pre-industrial magnetic cooling system for room temperature application," *Applied Energy*, vol. 98, pp. 556-561, 2012.

[19] K. Engelbrecht, D. Eriksen, C. Bahl, R. Bjørk, J. Geyti, J. Lozano, K. Nielsen, F. Saxild, Smith and N. Pryds, "Experimental results for a novel rotary active magnetic regenerator," *International Journal of Refrigeration*, vol. 35, pp. 1498-1505, 2012.

[20] T. Gottschall, A. Gràcia-Condal, M. Fries, A. Taubel, L. Pfeuffer, L. Mañosa, A. Planes, K. P. Skokov and O. Gutfleisch, "A multicaloric cooling cycle that exploits thermal hysteresis," *Nat Mater*, vol. 17, no. 10, pp. 929-934, 2018.

[21] F. Scheibel, T. Gottschall, A. Taubel, M. Fries, K. P. Skokov, A. Terwey and W. Keune, "Hysteresis Design of Magnetocaloric Materials—From Basic Mechanisms to Applications," *Energy Technology*, vol. 6, no. 8, pp. 1397-1428, 2018.

[22] L. F. Cohen, "Contributions to Hysteresis in Magnetocaloric Materials," *physica status solidi (b)*, vol. 255, no. 2, 2017.

[23] J. A. Barclay and W. A. Steyert, "Active magnetic regenerator". ENERGY United States, Department of US Department of Energy Patent US4332135A, 27 01 1981.

[24] H. Ucar, D. Paudyal and O. Boyraz, "Using numerical methods to screen magnetocaloric materials in an active magnetic regenerative cycle," *International Journal of Refrigeration*, vol. 120, pp. 50-57, 2020.

[25] J. Tusek, A. Kitanovski, S. Zupan, I. Prebil and A. Poredos, "A comprehensive experimental analysis of gadolinium active magnetic regenerators," *Applied Thermal Engineering*, vol. 53, pp. 57-66, 2013.

[26] J. Tušek, A. Kitanovski, I. Prebil and A. Poredoš, "Dynamic operation of an active magnetic regenerator (AMR): Numerical optimization of a packed-bed AMR," *International Journal of Refrigeration*, vol. 34, no. 6, pp. 1507-1517, 2011.

[27] U. Tomc, "Improvements to the heat transfer of an active magnetic regenerator," University of Ljubljana, Ljubljana, 2016.

[28] P. V. Trevizoli, A. T. Nakashima, G. F. Peixer and J. R. B. Jr., "Performance evaluation of an active magnetic regenerator for cooling applications – part I: Experimental analysis and thermodynamic performance," *International Journal of Refrigeratio*, vol. 72, pp. 192-205, 2016.

[29] P. V. Trevizoli, A. T. Nakashima, "Performance evaluation of an active magnetic regenerator for cooling applications – part II: Mathematical modeling and thermal losses," *International Journal of Refrigeration*, vol. 72, pp. 206-217, 2016.

[30] M. Zhang, O. Abdelaziz, A. M. Momen and A. Abu-Heiba, "A numerical analysis of a magnetocaloric refrigerator with a 16-layer regenerator," *Scientific Reports*, vol. 7, 2017.

[31] C. Aprea, A. Greco, A. Maiorino and C. Masselli, "Energy performances and numerical investigation of solid-state magnetocaloric materials used as refrigerant in an active magnetic regenerator," *Thermal Science and Engineering Progress*, vol. 6, pp. 370-379, 2018.

[32] S. Singh, L. Caron, S. W. D'Souza, T. Fichtner, G. Porcari, S. Fabbrici, C. Shekhar, S. Chadov, M. Solzi and C. Felser, "Large Magnetization and Reversible Magnetocaloric Effect at the Second-Order Magnetic Transition in Heusler Materials," *Advanced Materials*, vol. 28, pp. 3321-3325, 2016.

[33] A. G. Condal, "Giant caloric and multicaloric effects in magnetic alloys," Department de Física de la Matèria Condensada, Universitat de Barcelona, 2021.